Multiwavelength observations of GRB160625B by MASTER, Lomonosov, Konus-Wind and three stage collapse

V. M. Lipunov[1,2,*], V. A. Sadovnichy[3], M. I. Panasyuk[1,4], I. V. Yashin[4], S. I. Svertilov[1,4], D. Svinkin[5], E. Gorbovskoy[2], S. G. Simakov[2], G. V. Lipunova[2], V. G. Kornilov[1,2], D. Frederiks[5], V. Topolev[1,2], R. Rebolo[6], M. Serra[6] , N. Tiurina[2], E. Minkina[1,2], V. V. Bogomolov[1,4], A. V. Bogomolov[4], A. F. Iyudin[4], A. Chasovnikov[1,2], A. Gabovich[8], N.M. Budnev[7], O. A. Gress[2,7], G. Antipov[2], D. Vlasenko[1,2], P. Balanutsa[2], R. Podesta[5], K. Zhirkov[1,2], A. Kuznetsov[2], V. Vladimirov[2], F. Podesta[5], C. Francile[5], Yu. Sergienko[8], A. Tlatov[9], O. Ershova[7], D. Cheryasov[2] and V. Yurkov[8]

[1] *Lomonosov Moscow State University, Physics Department, Vorobievy Hills, 1, Moscow 119991, Russia*

[2] *Lomonosov MSU, SAI, Universitetsky, 13, Moscow 119234, Russia*

[3] *Lomonosov Moscow State Universit, GSP-1, Vorobievy Hills, 1, Moscow, 119991, Russia*

[4] *Lomonosov Moscow State University, Skobeltsyn Institute of Nuclear Physics (SINP MSU), Vorobievy Hills, 1, Moscow, 119991, Russia*

[5] *Ioffe Institute of theoretical physics, 26 Politekhnicheskaya, St Petersburg 194021, Russia*

[6] *Instituto de Astrofísica de Canarias, Lactea, E38205, LaLaguna, Tenerife, Spain*

[7] *Irkutsk State University, 20, Gagarin, Irkutsk 664003, Russia*

[8] *Blagoveschensk State Pedagogical University, Lenin, 104, Amur, Blagoveschensk 675000, Russia*

[9] *Kislovodsk Solar Station Pulkovo Observatory, Gagarina 100, Kislovodsk 357700, Russia*

**E-mail: lipunov@sai.msu.ru*

The detailed continuous fast optical photometry analysis obtained by MASTER Global Network for the GRB160625B optical counterpart MASTER OT J203423.51+065508.0 is presented. There are also hard X-ray and gamma-ray emission obtained by the Lomonosov and Konus-Wind spacecrafts detectors. We detected quasiperiodic emission components in the intrinsic optical emission of GRB160625B and propose a three-stage collapse scenario for this long and bright GRB. We associate quasiperiodic fluctuations with forced precession of a Spinar, i.e. self-gravitating rapidly rotating super dense body, whose evolution is determined by a powerful magnetic field. The spinar's mass lead it to collapse into a black hole at the end of an evolution.

Keywords: Gamma-ray burst

1. Introduction

Gamma-ray bursts (GRB) still remain a mysterious phenomenon. We proceed from the assumption believe that long gamma-ray burst occurs as a result of the collapse of the rapidly rotating core of a massive star. The fast rotation of the core slows down the collapse and extends time available to produce electromagnetic radiation. Two scenarios are possible here. In the first scenario (MacFadyen & Woosley, 2000),[1] a black hole first forms, and then the fallback of the supernova envelope, which has a supercritical torque, forms a heavy superdense disk. Due to the generation of magnetic fields by this disk, axial jets with a large gamma factor are generated, which we observe. In another scenario, a rapidly rotating magnetized object, a Spinar, is first formed, which is slowly compressed due to the dissipation of the rotational moment (Lipunov & Gorbovskoy, 2007).[2] In this case, a jet with a Poynting-Umov energy flow is formed along the rotation axis. The operating time of the central gamma-ray burst engine changes depending on the dissipation rate. In general, both scenarios require a fairly large torque in the collapsing stellar core. And here the authors are impressed by a binary scenario in which fast rotation occurs due to the tidal influence of the second component in a very close binary system (Tutukov & Cherepashchuk, 2016).[3] In this scenario, the centrifugal barrier is a consequence of the large torque acquired as a result of the natural evolution of the binary system. In the case of GRB160625B our attention was attracted by the quasiperiodic brightness fluctuations during the time of the central engine operation, and below we try to interpret them as a consequence of a Spinar Paradigm at work (Lipunova & Lipunov, 1997; Lipunov & Gorbovskoy, 2007;2008; Lipunova et al., 2009)[2, 4–6]

In this paper, we present multiwavelength observations of GRB160625B, one of the brightest gamma-ray bursts in the history of their study. We have concentrated on the temporal behavior of itsintrinsic electromagnetic radiation. We present optical and gamma-ray data, recorded during the time of the operation of the central engine of GRB160625B. We made an attempt to find traces of the duality of the GRB system. We have suspected traces of the dual nature of long GRBs. Of course, we do not have one hundred percent proof of this scenario, but this study can serve as an example of searching for and finding the dual nature of long GRBs.

2. Observations

GRB160625B was observed by the large number of space and ground telescopes in a wide range of electromagnetic waves from gamma-ray to radio. For the first time in the GRB study history, the polarization of its own prompt optical emission synchronous with the gamma one was discovered (Troja et al., 2017a).[7] Now we present the details of synchronous observations in the optical (MASTER OT J203423.51+065508.0) and gamma-ray ranges.

GRB 160625B triggered Fermi observatory at 2016-06-25 22:40:16UT , firstly as a short pulse (Fermi-GBM trigger 488587220, Burns et al.2016),[8] then the

Fermi-LAT triggered (Dirirsa et al. 2016)[9] at 22:43:24.82UT, at 22:51:16.03 Fermi-GBM triggered again (trigger 488587880).The GBM light curve consists of multiple peaks over approximately 700 seconds, the first one being 1 second long soft peak. The main peak, corresponding to the LAT trigger, was very hard and about 25 seconds long. The peak that triggered GBM for the second time was soft and about 30 seconds long (Burns et al. 2016).[8] Swift has initiated a series of observations and discovered uncatalogued X-ray sources at R.A.,Dec.(2000)=20:34:23.25 +06:55:10.5 with an uncertainty of 3.8 arcsec (Melandri et al. 2016), publishied it at 2016-06-26 06:54:13UT.

This long, extremely bright GRB 160625B also triggered BDRG detectors on-board Lomonosov Space Observatory of Moscow State University (Sadovnichii et al. 2017)[10](Fig. 1) and Konus-Wind at 22:40:19.875UT (Svinkin et al. 2016)[11](Fig. 1) as well as the CALET Gamma-ray Burst Monitor (CGBM) at 22:40:15.49 (Nakahira et al. 2016).[12]

The optical counterpart was discovered by RATIR (Troja et al. 2017b)[14] starting 8.53h after LAT trigger. MASTER started observation in polarization filters (Lipunov 2010, 2019, Kornilov 2012)[17–19] 31 sec after GBM notice time (57 sec after GBM, i.e. 131 sec before LAT Trigger, Dirirsa et al.2016)[9] at 2016-06-25 22:41:13UT (Gorbovskoy et al. 2016),[20] but published the circular in GCN (Barthelmy et al. 1998ab)[21, 22] at 16/06/28 14:05:38. The GCN publication was delayed by the installation of the new MASTER telescope in Argentina at this time (MASTER-OAFA). MASTER measurements probed the structure of the magnetic field at an early development stage of the jet, closer to a central black hole, and show that the prompt emission phase is produced via fast-cooling synchrotron radiation in a large-scale magnetic field that was advected from the black hole and distorted by dissipation processes within the jet (Troja et al. 2017a).[7] The optical data obtained by MASTER telescopes-robots (Lipunov et al. 2010,2019)[17, 18] have the best temporal resolution with the minimum exposure time of 5 seconds. This resolution made it possible to suspect quasiperiodic variability in the optical range, which we try to associate with the dual nature of the long GRB.

The detection of a substantial (8.3 ± 0.8 per cent from our most conservative estimation) variable linear polarization of a prompt optical flash that accompanied the extremely energetic and long prompt γ-ray emission from GRB 160625B was discovered by MASTER (Gorbovskoy et al. 2016a, Lipunov et al. 2016a, Troja et al. 2017a).[7, 15, 16]

2.1. *MASTER*

MASTER Global Robotic Net of Lomonosov Moscow State University in 2016 consisted of orbital MASTER-Shok detectors on-board Lomonosov spacecraft and of 8 ground observatories with identical scientific equipment distributed all over the Earth: MASTER-Amur, -Tunka, -Ural, -Kislovodsk, -Tavrida in Russia, -SAAO (South African Astronomical Observatory), -IAC (Tenerife, Spain, Teide observatory of Institute of Astrophysics of the Canary Islands), -OAFA (Argentina, San Juan National University Astronomical Observatory named by Felix Aguilar), see Lipunov 2010, 2019[17,18](Fig. 1). Identical equipment includes twin wide-field (MASTER-II, 4-8 square degrees up to 20m unfiltered limit at 180s exposition) and very wide field (MASTER-VWFC, 800 square degrees, up to 15m at summary image) optical channels (Kornilov et al. 2012)[19] which allows us to follow a target 24h per day in one photometric channel. MASTER-VWFC are the ground-based analogue of the MASTER-SHOCK cameras, that were installed on board the Lomonosov space observatory (Sadovnichy et al. 2017,2018, Lipunov et al. 2018, Svertilov et al.2018, Park et al. 2018).[10,23,25,37,38] Observations by MASTER-VWFC are unfiltered.

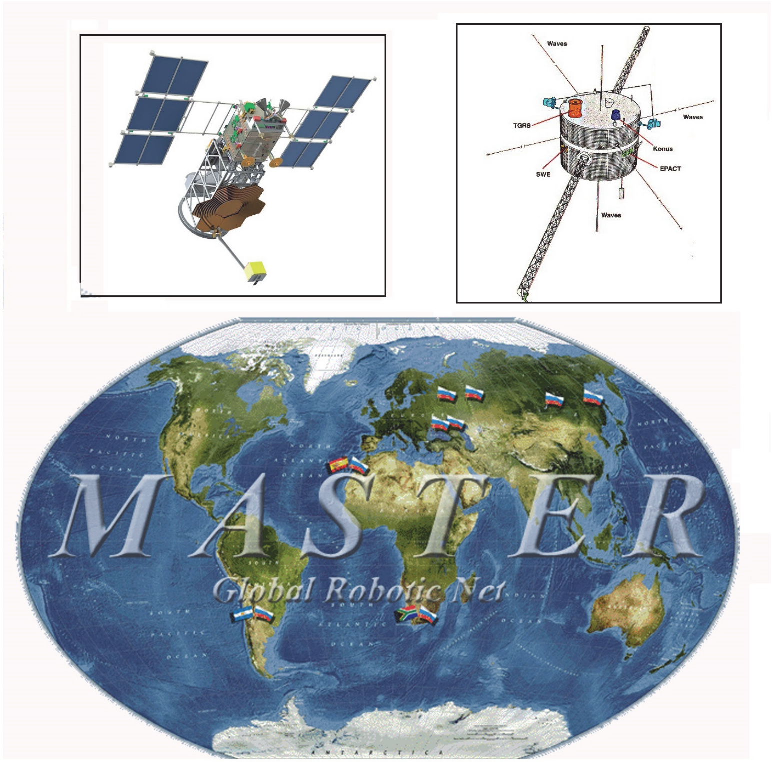

Fig. 1. MASTER Global Robotic Net. The upper left part shows Lomonosov satellite and the upper right part shows Konus-Wind. The flags indicate equipped sites of network stations.

MASTER own developed photometer can observe simultaneously in 2 orthogonally oriented polarization filters in both tubes of twin MASTER telescope

(Kornilov et al. 2012)[19] or in BVRI filters and unfiltered. Mount has fast positioning with the speed up to 30 deg/s.

MASTER key factors is own software for real-time reduction. It includes full robotization of all processes: hardware control, weather control, efemerides, central planner, automatic evening/morning calibration,and primary image reduction, astrometry and photometry, extraction of new optical sources and notification of the main station of them). Such features let us to discover significant and variable linear polarization during the prompt optical flash of GRB 160625B (Troja et al. 2017a),[7] to discover GRB optical counterparts (Lipunov et al. 2016, Gorbovskoy et al. 2016, Sadovnichy et al. 2018, Laskar et al. 2019),[20, 24–27] to discover Smooth Optical Self-similar Emission of GRB subclass (Lipunov et al. 2017),[28] to make the most optical support to GW150914 event (Abbott et al. 2016ab, Lipunov et al. 2017,2018),[29–31] to independently discover Kilonova GW170817(Abbott et al. 2017, Lipunov et al. 2017),[32, 33] to make the most optical support to the follow-up of a rare IceCube neutrino multiplet (Aartsen et al. 2017),[34] to discover V404Cygni polarization variability (Lipunov et al. 2017),[35] to make optical observationsthat revealed a strong evidence for a high-energy neutrino progenitor - blazar TXS 0506+056 for IC170922A (Lipunov et al. 2020)[36] , to discover more than 2000 optical transients of 10 different types and other.

2.2. *MASTER GRB160625B observation*

MASTER-IAC robotic telescope pointed to the GRB 160625B at 2016-06-25 22:41:13UT, and observed Swift X-ray error box (Melandri et al., 2016)[13] by MASTER-IAC wide field camera with a 5 second exposition time without filter and imaged several thousand frames.

MASTER-Tavrida started first frame exposition 12 seconds after LAT notice time (66s after trigger time) at 22:44:30UT.

MASTER-Tavrida and MASTER-IAC very wide field of view cameras (VWFC) observed GRB error-box when the Fermi-LAT detected the main impulse of GRB with a high coordinate accuracy of 0.5 degrees, 131 seconds after the first message.

MASTER OT J203423.51+065508.0 optical counterpart was detected at 22:43:30UT (+2.5 sec of exposition) UT with m_{OT}=8.60 and was getting brighter up to a maximum of 7.86m(see Fig. 2). The prompt optical emission strongly correlated with Konus-Wind gamma ray light curve (Svinkin et al., 2016).[11]

MASTER-IAC robotic telescope started observation of the error box 43 sec after LAT notice time or 95 sec after trigger time at 2016-06-25 22:44:59UTby main MASTER-II telescope in two polarizations. The OT was 8.6m at the moment.

As a result, MASTER not only registered the entire event of the GRB explosion in the optical range with the best time resolution (2.5 sec), but for the first time in the history of gamma-ray burst research, it detected the polarization of prompt optical emission from the gamma-ray burst while the flash was still going on (Troja et al. 2017a).[7]

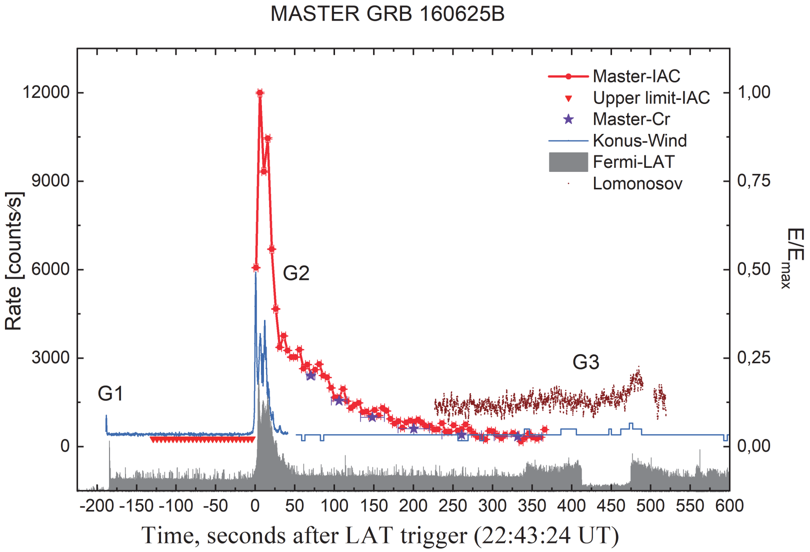

Fig. 2. Red curve - observations of the very wide-field MASTER-IAC cameras, reduced to the proper time of the system (compression of the burst time scale relative to the observed one). The purple dots corresponds to the MASTER-Tavrida measurements taken with a lower temporal resolution. The gray curve corresponds to the emission detected by Fermi-LAT (see Toja et al. 2017a.[7]

The gamma-ray burst GRB160625B turned out to be one of the most powerful cosmic explosions of this type, which appeared as a narrow jet of relativistic particles accelerated by the electromagnetic field of a rapidly rotating black hole at the other end of the Universe forming before our eyes.

An analysis of the MASTER's polarization observations made it possible for the first time to detect the polarization of GRB's intrinsic optical radiation and directly showed that the muzzle of the most powerful space gun was formed by an ordered powerful magnetic field of a forming black hole (Troja et al., 2017).[7]

This magnificent astrophysical experiment succeeded thanks to the interaction of scientists from several countries, who created unique robotic equipment to detect gamma rays, infrared radiation, and photons in the optical range born by the GRB event.

2.3. *LOMONOSOV Observations*

The GRB monitor (BDRG) aboard the Lomonosov (Sadovnichii et al. 2017)[10] observatory (hereafter BDRG/Lomonosov (Svertilov et al., 2018)[37] was built for the early detection of GRBs in the gammas of 0.01-3.0 MeV energy range and for generation of triggers for those events. The BDRG consisted of 3 identical detector units connected to the electronic unit. The BDRG instrument detector units (blocks) were mounted on the spacecraft payload platform in such a way that their axes are oriented 90° to each other. Each detector has a cosine angular dependence for a sensitive area not shaded by satellite construction elements within $\sim 60^\circ$ of its axis. The monitor's central axis, relative to which the detector axes are inclined, is directed toward to the local zenith. Thus, the total field of view for all three detectors is about 2π sr; and one quarter of this field, i.e. $\pi/2$ sr, is the value of a solid angle, within which limits the GRB position error can be estimated with sufficiently good accuracy through the comparison of all three detector outputs.

BDRG operates in two main observational modes: the monitor or continuous mode, and the burst mode. In the monitor mode all instrument outputs were recorded and stored continuously with time resolutions adjustable by commands from Earth. On the other hand, the burst mode was activated by on-board instrument triggers to record detailed information of each photon during the before-burst, burst, and after-burst time intervals. The BDRG trigger initiated the estimation of GRB positions and relayed the trigger not only to other GRB observation instruments onboard the Lomonosov spacecraft, i.e. SHOK optical cameras (Lipunov et al., 2018)[23] and Ultrafast Flash Observatory (Park et al., 2018),[38] but to the ground telescopes as well through the Gamma-ray Coordinates Network (GCN, Barthelmy et al. 1998ab)[21] viathe Global Star transmitter.

Each BDRG detector unit consisted of a thin layer (0.3 cm) of NaI(Tl) crystals optically coupled to a considerably thicker layer (1.7 cm) of CsI(Tl) crystals situated underneath. The diameter of the detectors is 13 cm, and both layers are read by a single photomultiplier tube (PMT). Thus, the overall detector area is about 130 cm2. The thickness of the NaI(Tl) layer is optimized for the soft part of energy range, and the working ranges of the units are 0.01-0.5 MeV for the NaI(Tl) layer and 0.05-3 MeV for CsI(Tl). As such, the NaI(Tl) layer serves as the main detector for hard X-ray timing, while the CsI(Tl) operates as an active shield against background gamma-rays. Additionally, the CsI(Tl) crystals can also detect gamma-rays with energies up to a few MeV. The difference in decay times for the NaI(Tl) ($\sim$0.25 ms) and CsI(Tl) ($\sim$2.0 ms) crystals permits the separation of light flashes in the scintillators through special electronic circuits that differentiate pulse shapes.

The information provided by the BDRG units consisted of a number of different categories for the data frames generated continuously (continuous mode) as well as irregularly by various triggers (burst mode). The continuous data stream included three types of frame corresponding to the instruments' monitoring, spectrum, and event. Monitoring frames provided count rates in 8 energy channels for the NaI(Tl) and CsI(Tl) scintillator crystals for each of the BDRG detector units, while spectrum frames contain 724 channel spectra for NaI(Tl) and CsI(Tl), separately. Event frames gave the primary values for energy release within the NaI(Tl) and CsI(Tl) crystals, combined with time data for a fixed number of detected gamma-quanta. Likewise, information about the main parameters for all GRB triggers was stored and transferred in the form of "trigger logs". There are three trigger types categorized as "fast," "slow" and "super-slow," with characteristic times of 10 ms, 1 s, and 20 s, respectively. Corresponding to each trigger type, three data frame sequences for the monitoring, spectrum, and event were generated continuously in a manner similar to the continuous mode discussed above. A portion of data collected before the trigger was always included for all trigger types.

On 25 June 2016 near the GRB160625B trigger, the BDRG/Lomonosov operated in monitoring mode. The background environment at the time of event was very complicated. The Lomonosov satellite was flying through the radiation belts.

The count rate variations in the BDRG/Lomonosov gamma-quanta channels are illustrated by the curves in the upper panel of Fig. 3, in which count-rates of three BDRG-1 NaI detector channels 10 – 35, 35 – 170, 170 – 650 keV shown with the time resolution of 0.1 s are plotted. Full data is available on the link(http://master.sai.msu.ru/static/MG16MASTER/BDRG160625B.txt)

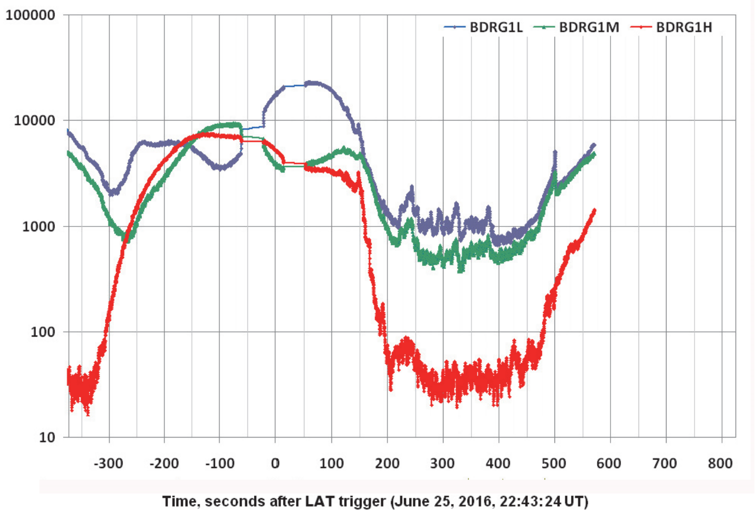

Fig. 3. GRB160626B γ-ray light curves.The BDRG-1(NaI detector) counts vs time in the 10-35keV (BDRG1L), 35-170 keV (BDRG1M), 170-650 keV (BDRG1H) ranges.

The clear count-rate increases in the time interval from about -150 to 350 seconds relative to the Swift trigger time (-300 to 200 seconds relative to the LAT trigger time) corresponds to the satellite crossing outskirts of the external radiation belt. After that the satellite flew into the region of the South polar cap, where the background is smaller, and after that it began to cross the outer belt again and the background began to increase. Thus, due to such background variations the main pulse (G2) as well as the precursor (G1) could not be observed on by the

Lomonosov satellite detectors. Only the "last tail" (G3) could be observed. However, during the corresponding time interval (from about 350 to 550 seconds from LAT trigger time) count variations in the BDRG/Lomonosov were in reality combination of GRB counts plus variations caused by unstable electron fluxes in the polar cap. The last component can give the significant input in gamma ray channels of the instrument due to electron bremsstrahlung. Thus, to obtain the real GRB light curve it is necessary to clean the detector outputs from electron background variations.

To realize this procedure we used the outputs from different BDRG detectors. Because of different BDRG detector orientation the given GRB source was observed by separate detectors at different angles. In the case of GRB160625B only BDRG1 detector unit was illuminated, the angle between the detector axis and direction toward the GRB source was about 56°, while for BDRG2 and BDGR3 these angles were about 136° and 116° respectively. It means that GRB source was out of field of view (FOV) of both latter detector units. On the other hand, since counting rate of the irregular variations observed in the polar cap regions are mainly due to the quasi-trapped electron fluxes having an anisotropic but rather wide pitch-angle distribution, they will exhibit similar temporal behavior in separate, although differently oriented detectors. It allows us to use regression analysis of detector unit count rates obtained for two detectors during time interval of GRB observation to estimate regression coefficients, which then can be used for rejection of the part of counting rate variations caused by electron fluxes. Because during the time of GRB160625B observation BDRG2 unit was switched-off, for regression analysis only the BDRG1 and BDRG3 unit outputs were used. To be exact, we selected time interval from 200 to 450 seconds after LAT trigger (22:43:24UTC) to estimate regression coefficients, which corresponds to the time between G2 and G3 events, when expected input to detectors counting rates from GRB160625B was negligible.

2.4. ***Konus-Wind observations***

GRB 160625B triggered Konus-Wind GRB spectrometer (KW, Aptekar et al. 1995)[41] at T0= 81619.875 s UT (22:40:19.875; Svinkin et al., 2016).[11] The burst was detected by the S2 detector, which observes the Northern ecliptic hemisphere; the incident angle was 65.2 deg. The propagation delay from Earth to WIND is 3.356 s for this GRB; correcting for this factor, the KW trigger time corresponds to the Earth-crossing time 81616.519 s UT (22:40:16.519).

2.4.1. *Time history*

Count rates for Konus-Wind are recorded in three energy bands in the triggered mode: 17–70 keV (B1), 70–300 keV (B2), and 300–1170 keV (B3). The record starts at T0 - 0.512 s and continues to T0 + 229.376 s with an accumulation time varying from 2 to 256 ms. Waiting-mode count rate data are available up to T0 + 250 s in the same energy bands with a coarse temporal resolution of 2.944 s. A source activity after time interval T0 + 250 s may be traced in the housekeeping mode with temporal resolution of 3.68s for the 70–300 keV energy range.

The prompt-emission light curve (Fig. 4) can be divided into three episodes. It starts, at ∼ T0 - 0.3 s, with a short, spectrally-soft initial pulse (precursor) which has duration of about 1 s. The precursor is followed, starting at ∼ T0 + 180s, by the main, extremely bright and spectrally-hard emission episode lasting for about 40 s. The final episode observed by KW in the housekeeping mode starts at ∼ T0 + 530 s and has duration of about 150 s. The total burst duration is about 680 s.

The first episode was localized only by Fermi (GBM) with a position uncertainty of about 2 deg (statistical only). The difference in the arrival time of the gamma-ray signals at Fermi-GBM and Konus-Wind provides additional significant constraints on the gamma-ray localization of the episode (Zhang et al., 2018).[42] The triangulation of the first episode is consistent with the source position determined by Swift-XRT in the main episode, supporting the association of the precursor and the burst.

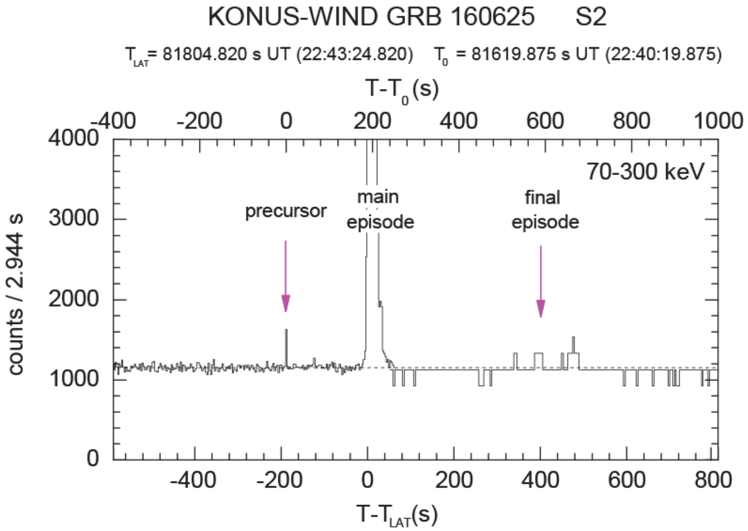

Fig. 4. GRB 160625B light curve recorded in the KW waiting and housekeeping modes in the 70-300 keV band (B2).

Let us discuss the time-resolved spectral analysis. In the triggered mode, Konus-WIND measures 64 energy spectra in 128 channels of two overlapping energy bands: 20–1170 keV (PHA1) and 244 keV–15 MeV (PHA2). The first four spectra have a fixed accumulation time of 64 ms; after that, the accumulation time varies over 0.256-8.192 s, depending on the current intensity of the burst. Five initial energy spectra covered the precursor (T0 – T0+8.448 s) and 35 covered the main episode (T0+180.480 - T0 + 237.824 s).

The spectral analysis was performed with XSPEC version 12.9.0i (Arnaud 1996)[43] with the three model: Band GRB function (Band et al. 1993):[44] $f(E) \sim E^{\alpha} exp(-(2+\alpha)E/Epeak)$ for $E < Epeak(\alpha - \beta)/(2+\alpha)$, and $f(E) \sim E^{\beta}$ for $E > Epeak(\alpha - \beta)/(2+\alpha)$, where α is the power law photon index at low energies, Epeak is the peak energy in the EF(E) spectrum, and β is the high-energy photon index; a cutoff power law model (CPL): $f(E) \sim E^{\alpha} exp(-(2+\alpha)E/Epeak)$; and a simple power law. The spectral models were normalized to the energy flux in the 20 keV – 10 MeV range, a standard band for the KW GRB spectral analysis.

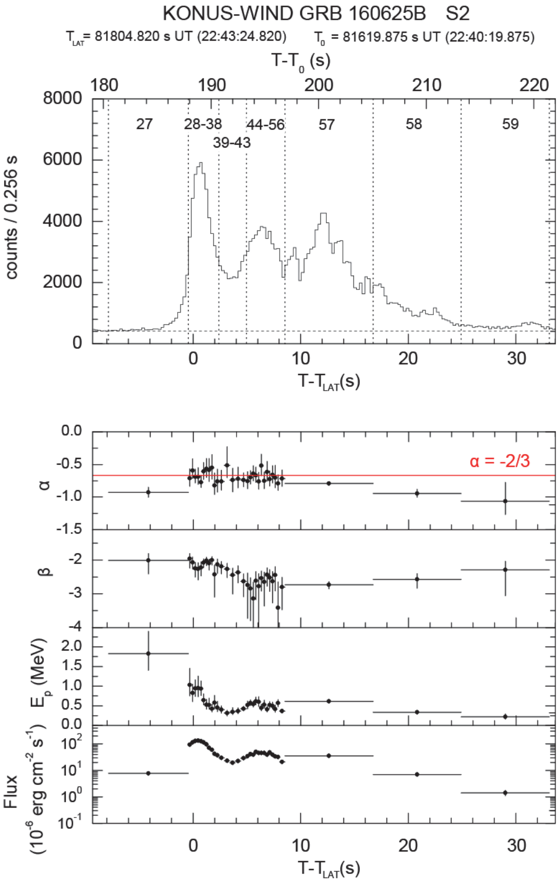

Fig. 5. Spectral evolution of the gamma-ray emission during the prompt phase of the burst main episode. The Konus-WIND light curve in the combined B1+B2+B3 energy band (17-1170 keV) is shown with 256 ms resolution, along with the temporal behavior of the Band spectral model parameters Epeak, α, and β obtained from the time-resolved fits.

Typically, the spectral channels are rebinned to have at least 10 counts per energy bin to ensure Gaussian-distributed errors and the correctness of the χ^2 statistic.

For the precursor, constrained spectral parameters of the CPL model are available only for the sum of the first four spectra, while for the main episode, a good count statistic is achieved for 35 individual spectra between T0+180.480 s and T0+237.824 s, the spectrum between T0+ 229.632 s and T0+237.824 s is well described by a simple power law. The good spectral coverage enables us to construct the temporal behavior of the model parameters (α, β, Epeak) and to trace in detail the evolution of the spectral composition of radiation over the course of the main episode (Fig. 5).

Spectrum 27 was measured at the onset of the very intense initial pulse of the main episode (Fig. 5). The emission at this moment is hard; Epeak reaches the highest value for the burst ($\sim$ 1.8 MeV). After the summit of the brightest pulse, Epeak starts to decrease gradually (spectra 28-38), down to $\sim$ 300 keV in spectra (39-43), and then grows up to $\sim$ 600 keV at the time of the second peak (spectra 44-56), staying at this level during the last peak (spectrum 57). Spectra 58-60 describe the decay of the main episode showing the typical decrease in Epeak. During the brightest part of the main episode the low-energy spectral index is approximately constant and is consistent with the synchrotron emission in the slow-cooling regime $\alpha = -2/3$ (Preece et al., 1998).[45] The high-energy index β shows no significant correlation with energy flux and is typical for long GRBs ($\beta \sim$ -2).

Spectrum 1-4 (time –averaged), corresponding to the peak of the initial pulse is well fitted with a CPL model with $\alpha \sim$ -0.4, and Epeak $\sim$ 70 keV ($\chi^2/dof =$ 16.5/29). The fit with a single blackbody (BB) component yields kT= 17.3 (-1.6, +1.6) keV, energy flux 1.92 (-0.19,+0.19) $10^{-6} erg/cm^2/s$, with $\chi^2/dof = 32.1/30$; the fit underestimates count rate at energies below $\sim$ 30 keV. Thus, despite the BB kT is consistent with the value found by Zhang et al., 2018,[42] we argue that BB model cannot be favoured for the spectrum.

3. Modeling

Looking at the optical light curve starting from 20 seconds relative to the main pulse and up to 200 - 250 seconds, one can suspect quasiperiodic brightness oscillations with an amplitude significantly exceeding the random brightness measurement error. Recall that a five-second exposure on ultra-wide field cameras is practically without delay. Such variability at times of the order of ($\tau \sim$ 10-20 seconds) is caused by internal physical processes in the operation of the central engine. However, it would be tempting to associate this phenomenon with the interaction of a relativistic jet with quasiperiodic inhomogeneous layers in the radial distribution of the progenitor's stellar wind. This type of inhomogeneity can be caused by the presence of a close second component in the collapsing star's binary system. Calculations carried out earlier (Lipunova et al. 2009)[6] show that in systems with an orbital period of less than 1 - 2 hours, tidal forces lead to a critical increase in the spin moment of the collapsar. As a result, it is under these conditions that the formation of a massive accretion disk (Woosley 1993)[46] or a spinar (Lipunov & Gorbovskoy, 2007)[2] prolongs the magneto-rotational collapse, which leads to the phenomenon of a gamma-ray burst.

First of all, we will discuss the possible reasons for the quasiperiodic optical emission, which is an intrinsic emission at the stage of the central engine operation and must reflect some quasiperiodic oscillations of the central engine. This circumstance is supported by the fact that we detect oscillations after 30 seconds (in our own frame of reference) from the trigger, that is, at the same time when the optical and gamma spectra become one. Recently, Suvorov and Kokkotas (2021)[47] discussed quasiperiodic pulsations of X-rays from some short GRBs in the magnetar model. Actually, the only property of the magnetars used here is the one inherent to all radio transmitters they loose energy approximately according to the magnetic dipole law (Pacini, 1967)[48] and their total power changes over time $L \sim t^{-2}$. In connection with the gamma-ray bursts, this circumstance was expressed by Lipunova & Lipunov (1998).[4] The merit of the works of Suvorov and Kokkotas (2021)[47] is the attraction of the idea that the observed quasiperiodic oscillations are associated with the free precession of a neutron star with an anomalously strong magnetic field. In fact, the magnetar model is only a special case of a more general model of the magnetorotational collapse - Spinar Paradigm (Lipunov & Lipunov, 1998; Lipunov & Gorbovskoy, 2007, 2008; Lipunova et al., 2009).[2, 4–6] In the framework of Spinar Paradigm, it is assumed that the initial rotational moment of the body is so great that centrifugal forces have a significant effect on the collapse process. In particular, this model successfully explains not only the plateau phenomenon, but also a sharp (by several orders of magnitude) cliff at the end of the plateau (Lipunov & Gorbovskoy, 2007).[2] In fact, an approximate non-stationary model of gravitational-rotational collapse (Lipunov & Gorbovskoy, 2008)[5] includes all relativistic effects plus the contribution of the nuclear forces of the neutron liquid. The collapse character depends on three main parameters: the core mass M of the collapsing star, the generalized Kerr parameter $a_0 = I\omega_0 c/GM^2$ and the ratio of magnetic and gravitational energy $\alpha_m = U_m/U_{gr} << 1$ which remains constant in the approximation of the conservation of the magnetic flux. A black hole or a neutron star can also be the end product of the collapse (Lipunova et al., 2009).[6] In the process of formation of both types of objects, an intermediate object is formed - a spinar - which can experience not only free, but also forced precession. In addition, if a neutron star can only slow down, decreasing the overall luminosity, the spinar can accelerate as it evolves, and this will even be accompanied at certain stages by an increase in luminosity. It is precisely by the spinar precession that we propose to explain the suspected oscillations of the intrinsic optical emission of the GRB160625B gamma burst. Remarkably, the magneto-rotational collapse model naturally explains the existence of the precursor, with which we begin.

In the spinar model, the precursor of the gamma-ray bursts occurs during the first abrupt stop of the collapse due to the increase in centrifugal force (Fig. 6).

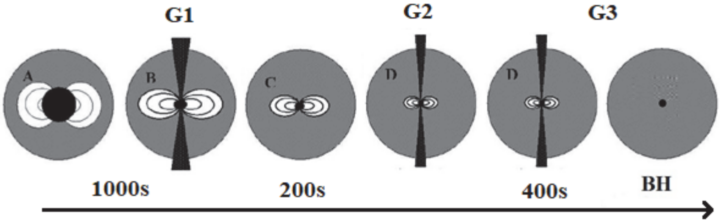

Fig. 6. Scheme of the three-stage magneto-rotational collapse in the Spinar Paradigm.

At this moment, half of the gravitational energy accumulated by the free-falling progenitor core is converted into heat. The second half of the work of gravitational forces turns into the energy of the spinar rotation. In other words, the centrifugal forces stop the collapse and a spinar is formed - which continues to slowly contract, losing its extreme moment and constantly increasing its radiation power (see Fig. 6). This is the formation of the precursor! Its maximum power $E_{precursor} \approx GM^2/2R_{sp}$ is determined by the radius of the formed spinar (Lipunov & Gorbovskoy, 2007)[2] $R_{sp} \approx a_0^2 R_g/2$, where R_g – Shwarcshild radius:

$$E_{precursor} \approx GM^2/2R_{sp} \approx (1/2a_0^2)Mc^2 \tag{1}$$

If the core torque is not too high $a_0 < 5 - 10m^{-1} (m = M/M_0)$, then this energy directed mainly along the spinar rotation axis will pierce the progenitor shell and we will see the precursor (Lipunov & Gorbovskoy, 2007).[2] However, immediately after the formation of the Spinar, the energy released by the spinar will already be determined by the magnitude of the magnetic energy $L_{sp} = U_m \omega \approx \alpha_m U_{gr} \omega$. Accordingly, the energy released by the spinar in one spin period and the corresponding pressure impulse on the shell will be reduced by a factor of $\alpha_m << 1$, hence the jet breakdown will happen. But if the torque is lost, the luminosity of the spinar will grow $L_{sp} = U_m \omega \approx \varepsilon_m U_{gr} \omega$ and finally break through the shell. This will be the time close to the beginning of the gamma-ray burst t_{GRB}. However, the time elapsed from the precursor to the start of the gamma-ray burst will be determined by the rate of loss of the spinar torque at the moment of its formation:$\Delta t \approx I\omega/U_m$. We can express the magnetic energy through the magnetic flux $\Phi = \pi B R^2 = \Phi_{28} 10^{28} Gs\, cm^2$, thus normalizing the flux to the characteristic of magnetars the does not change during the collapse, according to our assumption. Then we get the precursor time:

$$\Delta t_1 \approx -800s\, \Phi_{28}^{-2} m_{10}^3 a_0^3 \tag{2}$$

Kerr Black Hole released energy can reach 44% (Kip Thorne, 1974),[49] we get another important ratio of precursor fluence to gamma-ray burst fluence $E_{pre}/E_{GRB} \approx a_0^{-2}$. Usually there is a ratio $E_{pre}/E_{GRB} \approx 1 - 10\%$ (Troja, 2007),[50] corresponding to the generic Kerr parameter $a_0 \sim$ 3-10 . For the masses of nuclei close to M $\sim M_{OV}$, a larger Kerr parameter is required. However, in this case, it is necessary to include the contribution of nuclear forces (Lipunova et al., 2009).[6]

After the formation of the spinar, the direction of the magnetic flux of course does not have to coincide with its axis of rotation. We recall that we are considering the case of the conservation of the magnetic flux without an accompanying generation of the type of the dynamo mechanism. Therefore, a spinar can participate in a free precession, especially when it turns into a magnetar. However, a spinar is not a neutron star, whose surface is a hard boundary, beyond which there is a vacuum, or a highly discharged magnetosphere with a Julian-Goldreich density (Lipunov, 1992).[51] Spinar is an idealization of a superdense rotating body surrounded by a gas-dynamic plasma. Its evolution can be described by the equation:

$$dI\omega/dt = K_{\parallel} + K_{\perp} \tag{3}$$

On the right is the moment of forces, the parallel component of which leads to a change in the spinar's rotational moment in magnitude, and the perpendicular component leads to forced precession. It is clear that the spinar is not a rigid body, but the experience of studying the precession of accretion disks under the action of the magnetic moments of the seat shows that even thin disks successfully precess, though in a differential way (Lipunov & Shakura, 1980).[52] The maximum value of both moments of forces in equation 3 is determined as $|K| \approx U_m = \varepsilon_m U_{gr}$. The forced precession frequency turns out to be of the order of $\Omega = |K_{\perp}/I\omega| \approx \varepsilon_m \omega$. As the spinar radius approaches the event horizon $R \to R_g/2$ spinar frequency tends to the $\omega \to c/R_g$ as $R \to Rg$. So far as $U_m \to \varepsilon_m M c^2$ we get an estimate of the precession period:

$$T = 2\pi/\Omega = (2\pi/\omega)\varepsilon_m^{-1} \approx 5000s\,\Phi_{28}^{-2} m_{10}^3 r^{3/2} \tag{4}$$

Here $r = R/Rg$.

For the precursor GRB160725B in its own frame of reference $\Delta t_{pre} \approx -70s$ (we took z = 1.406 (GCN circular №19600), and the characteristic time of variations is T $\approx$ 10 sec. From 2 and 4 we obtain the estimate $a \approx 10$ and $\Phi_{27}^{-2} m^3$. Accordingly, the magnetic flux turns out to be quite reasonable $\Phi_{27}^{-2} \approx 140 m^{3/2}$.

After the main pulse (G2), the luminosity of the spinar begins to decrease. This is a sure sign that the role of nuclear forces is becoming important. The role of nuclear forces can become important only if the mass of the collapsing nucleus does not greatly exceed the Oppenheimer-Volkov limit. Let us recall that the Oppenheimer-Volkov limit essentially depends on the contribution of centrifugal forces to the equilibrium of the neutron star. So if the fraction of the rotational energy in the virial theorem is 10-20%, the Openhemer Volkov limit can increase by 2-3 times, depending on the equation of state of the neutron star (Lipunov, 1992).[51] With a mass of 4-5 solar masses, the spinar will be supported by nuclear forces until it freezes. This will happen during the after

$$\Delta t_3 \approx I\omega/U_m \approx 6I\omega R/\Phi^2 \approx 10s\, m^2 \Phi_{27}^{-2} r^2$$

So far as $r \to 1/2$ relativistic effects should be taken into account immediately.

Next, we applied a dynamic model of gravimagnetic collapse, which allows us to describe the evolution of a collapsing spinar from the moment of the loss of stability to the collapse into a black hole (Lipunov & Gorbovskoy, 2008; Lipunova et al., 2009).[5,6] In this formulation, a simple non-stationary three-parameter model of collapse is obtained with the decisive role of the rotation and the magnetic field. The input parameters of the theory are the mass, angular momentum and magnetic field of the collapsar. The approximate model includes: centrifugal force, relativistic effects of the Kerr metric, pressure of nuclear matter, dissipation of angular momentum under the influence of a spinar magnetic field, decrease in the dipole magnetic moment as a result of compression and the effects of general relativity (a black hole has no hair), neutrino cooling, time dilation due to gravitational redshift.

In Fig. 7 the results of calculating our approximate model are shown, the parameters of which are given in Fig. 1. Obviously, the main time intervals between the events of the gamma-ray burst G1, G2, G3 are in good agreement with observations. Of course, we do not pretend to describe a detailed light curve within the framework of our approximate model. We can only compare with observations the total energy release of the central engine at times G1, G2 and G3.

Table 1. Core collapse with the mass $M = 3.52M_\circ, M_{OV} = 2.5M_\circ$, effective Kerr parameter $a_0 = 4.9$ and magnetic parameter $a_m = 10^{-4}$.

Stage	Time(obs),s	E(obs)/E90	Time,s	E/E90	R/Rg	B,Gs	a_0
G1	-180	0.02	-75	0.03	37	10^{13}	4.9
G2	0	0.88	0.93	2	3	$2 * 10^{14}$	2.4
G3	∼450	190	0.04	0.04	3	$1.2 * 10^{15}$	1

We associate a slight increase in the gamma flux in G3 with an increase in the power of the central engine at the moment when the spinar loses its stability and collapses into a black hole. Note that such a three-stage collapse occurs only when the mass of the collapsing nucleus exceeds but is comparable with the Oppenheimer – Volkov limit.

4. Discussion

We presented multi-wavelength observations of GRB160625B, one of the brightest gamma-ray bursts in the history of their study. The authors of the article have already published a paper, concerning the first in the history discovery of variable polarization of the intrinsic emission of gamma-ray bursts (Troja et al., 2017).[7] Here we have concentrated on the temporal behavior of itsintrinsic electromagnetic radiation and presented optical and gamma-ray data, recorded during the time of the operation of the central engine of GRB160625B. We made an attempt to find

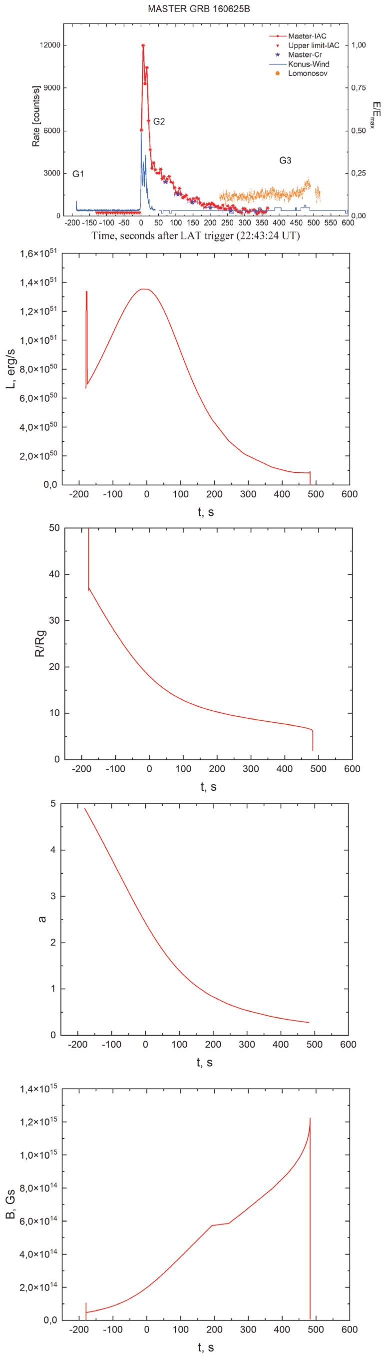

Fig. 7. In the diagram of the GRB160625B event in the observer's frame of reference is shown. In the top diagram, we have shown three principal G1 events - the position of the precursor ($\Delta t = -200$ s), the main peak of the G2 pulse ($t = 0$) and finally the last episode of increased G3 activity ($\Delta t = 400$–500 s).

traces of the duality of the GRB system, suspected traces of the dual nature of long GRBs. This study can serve as an example of searching for and finding the dual nature of long GRBs.

Long bright GRB160625B is rare, but not unique. GRB 080319B (Racusin et al., 2008)[53] also had a significant gap between the optical flux and the flux obtained by extrapolating the standard spectrum to the low frequency range. For GRB 080319B Kumar and Narayan (Kumar, Narayan 2009)[54] (see also Lazar et al 2009)[55] proposed a relativistic turbulence model to explain the fine structure of the light curve observed in the gamma range. It is assumed that the matter of the dropped shell is divided into two phases: the turbulent cells and everything in between. In this case, gamma emission is generated in both phases (reverse Compton), and synchrotron radiation of electrons in the inter-cell space is responsible for the radiation flux in the optics.

This explains a number of observed properties of gamma-ray bursts and, what is important in the context of this work, the huge excess of the flux in the optical range over what is dictated by the Band function. However, the natural consequence of this theory is a diminishing of the polarization over time, since the assumed turbulence entangles the magnetic field, leading to depolarization. In fact, the MASTER polarization observations (see Troja et al., 2017)[7] show an increase in polarization. Thus, in the case of GBR 160625B, the relativistic turbulence model does not work.

We interpret the features of the GRB160625B radiation within the framework of the model of a three-stage magnetorotational collapse of the core of a massive star whose mass exceeds but is comparable to the Oppenheimer-Volkov limit. In this model, the first G1 event in Spinar Paradigm will be explained by an abrupt stop of the nucleus collapse at the centrifugal barrier and the formation of a spinar. In this case, half of the accumulated gravitational energy is converted into rotational energy, and the second can be converted into jet energy along the spinar's axis of rotation. Further, as the rotational moment is lost, the spinar is compressing, gradually increasing its rotational energy, mainly emitted along the axis of rotation with a power of the proportional to the Umov-Poynting vector electromagnetic energy flow $E_{G1} = U_m \omega$. Of course, the observer will not see a smooth curve, since the jet must accumulate enough energy to pierce the progenitor shell (Lipunov & Gorbovskoy, 2007).[2] Naturally, in a model based on the conservation laws with an approximate description of the torque dissipation, one should not rely on the exact repetition of the light curve at the moment of the mainpulse G2. Therefore, we only achieved the coincidence of the moment of the maximum energy release with observations and the interval preceding the collapse of a heavy spinar with a powerful magnetic field and a mass exceeding the Oppenheimer-Volkov limit for a non-rotating neutron star.

MASTER and Lomonosov Space Observatory are supported by Lomonosov Moscow State University Development program (equipment). VL, PB are supported by RFBR grant 19-29-11011. NB is supported by FZZE-2020-0017).

References

1. MacFadyen A. I., Woosley S. E., 2001, ApJ 550, 410
2. Lipunov V., Gorbovskoy E., 2007, ApJ, 665L, 97L
3. Tutukov, A. V., Cherepashchuk, A. M., 2016, ARep, 60, 461
4. Lipunova G.V. and Lipunov V.M., 1998, A&A, 329, L29
5. Lipunov V., Gorbovskoy E., 2008, MNRAS, 383, 1397L
6. Lipunova G. et al. 2009, MNRAS,397,1695
7. Troja et al., 2017a, Natur, 547, 425T
8. Burns et al. 2016, GCN Circular, 19581,1
9. Dirirsa et al., 2016, GCN 19580, 1
10. Sadovnichii V., Panasyuk M. et al. 2017, SSRv, 212, 1705S
11. Svinkin et al. 2016, GCN, 19604, 1
12. Nakahira et al. 2016, GCN Circular, 19617,1
13. Melandri et al. 2016, GCN Circular, 19585,1
14. Troja et al. 2017b, GCN Circuar, 19588,1
15. Gorbovskoy et al. 2016a, GCN Circular, 19612,1
16. Lipunov et al. 2016a, GCN Circular, 19683,1
17. Lipunov V. et al. 2010, Advances in Astronomy, 2010, 30L
18. Lipunov et al. 2019, ARep, 63, 293L
19. Kornilov V. et al. 2012, ExpAst, 33, 173
20. Gorbovskoy et al. 2016b, MNRAS, 455, 3312
21. Barthelmy S. D. et al. 1998a, AIP Conference Proceedings, 428, 129
22. Barthelmy S. D. et al. 1998b, AIP Conference Proceedings,428, 99
23. Lipunov V. et al. 2018, Space Sci Rev, 214, 6
24. Lipunov et al. 2016b, ApJ, 833, 198L
25. Sadovnichy, V., Panasyuk M. et al. 2018, ApJ, 861, 48S
26. Ershova et al., 2020, ARep, 64, 126
27. Laskar et al. 2019, ApJ, 884, 121
28. Lipunov et al. 2017d, ApJ, 845, 52L
29. Lipunov et al. 2017a, MNRAS, 465, 3656L
30. Abbott B. P. et al. 2016, ApJL, 826, 13
31. Lipunov et al. 2018, NewA, 63, 48L GW
32. Abbott B. P. et al. 2017a, ApJL, 848, 12
33. Lipunov et al2017c, ApJL, 850, 1
34. Aartsen M. et al. 2017, A&A, 607A, 115I
35. Lipunov et al. 2019, NewA, 72, 42
36. Lipunov V. et al. 2020, ApJ, 896L, 19L
37. Svertilov S.I., Panasyuk M.I.et al. 2018, SSRv, 214, 1
38. Park I.H., M.I., etal.. 2018 Space Sci Rev, 214, 14
39. Mazaeva et al. 2016, GCN Circular, 19605, 1
40. von Kienlin et al.2003, A&A 411, L299-L305
41. Aptekar et al.. 1995,SSRv, 71, 265A
42. Zhang, B. et al. 2018, NatAstron 2, 69
43. Arnaud 1996 ASPC, 101, 17A
44. Band D.,1993, ApJ, 413, 281
45. Preece et al. 1998 ApJ, 506L, 23
46. Woosley, S. E. 1993, ApJ, 405, 273
47. Suvorov A.G., Kokkotas K.D., 2021, MNRAS, 502, 2482-2494
48. Pacini, F. 1967, Natur 216, 567-568

49. Kip S. Thorne 1974, ApJ, 191, 507-519
50. Troja, E., et al. 2007, ApJ, 665, 599
51. Lipunov V. M. 1992, Astrophysics of Neutron Stars, Springer
52. Lipunov V. M., Shakura N. I., SvAL, 6, 14L
53. Racusin, J.et al. 2008, Nature 455, 183
54. Pawan Kumar, Ramesh Narayan, 2009, MNRAS, 395 (1), 472
55. Lazar M., Poedts S. 2009, A&A, 494, 311-315